Original research

# Dynamic differences between DNA damage repair responses in primary tumors and cell lines

Collin Gilbreath [a], Shihong Ma [a], Lan Yu [a], Rajni Sonavane [a], Carlos M. Roggero [a], Anvita Devineni [a], Ryan Mauck [a], Neil B. Desai [b], Aditya Bagrodia [a], Ralf Kittler [c], Ganesh V. Raj [a,d,\*], Yi Yin [a,\*]

[a] *Department of Urology, University of Texas Southwestern Medical Center, Dallas, TX 75390, USA*
[b] *Department of Radiation Oncology, University of Texas Southwestern Medical Center, Dallas, TX 75390, USA*
[c] *Eugene McDermott Center for Human Growth and Development, University of Texas Southwestern Medical Center, Dallas, TX 75390, USA*
[d] *Department of Pharmacology, University of Texas Southwestern Medical Center, Dallas, TX 75390, USA*

## ARTICLE INFO

## ABSTRACT

The study of DNA damage repair response (DDR) in prostate cancer is restricted by the limited number of prostate cancer cell lines and lack of surrogates for heterogeneity in clinical samples. Here, we sought to leverage our experience with patient derived explants (PDEs) cultured *ex vivo* to study dynamics of DDR in primary tumors following application of clinically relevant doses of ionizing radiation (IR) to tumor cells in their native 3-dimensional microenvironment. We compared DDR dynamics between prostate cancer cell lines, PDEs and xenograft derived explants (XDEs) following treatment with IR (2Gy) either alone or in combination with pharmacological modulators of DDR. We have shown that following treatment with 2Gy, DDR can be consistently detected in PDEs from multiple solid tumors, including prostate, kidney, testes, lung and breast, as evidenced by γ-H2AX, 53BP1, phospho-ATM and phospho-DNA-PKcs foci. By examining kinetics of resolution of IR-induced foci, we have shown that DDR in prostate PDEs (complete resolution in 8 h) is much faster than in prostate cancer cell lines (< 50% resolution in 8 h). The transcriptional profile of DDR genes following 2Gy IR appears to be distinct between PDEs and cell lines. Pre-treatment with drugs targeting DDR pathways differentially alter the kinetics of DDR in the PDEs and cell lines, as evidenced by altered kinetics of foci resolution. This study highlights the utility of PDEs as a robust model system for short-term evaluation of DDR in primary solid tumors in clinically relevant microenvironment.

## Introduction

Current concepts of DNA damage response (DDR) in prostate cancer are largely derived from data from a small number of human prostate cancer cell lines and non-primate animal models [1–3], which represent unsatisfactory surrogates for the heterogeneity of primary prostate cancer clinical samples. In addition, the high doses of ionizing radiation (IR) (typically 5–10 Gy/fraction) used for these studies contrast with the most common clinically used 'conventionally' fractionated doses (1.8–2 Gy/fraction) and may erroneously highlight repair pathways that are only activated at high doses [4]. Further, prostate cancer cell lines in monolayer cultures lack the appropriate three-dimensional structure or stromal interactions that may modulate radio-responsiveness in the native human prostate microenvironment [5]. These findings strongly indicate the need for more biologically and clinically relevant models for understanding DDR of prostate cancer.

In our laboratory, we have developed a rapid and cost-effective patient derived explants (PDEs) *ex vivo* culture technique for evaluating the therapeutic response of fresh tissues from extirpated surgical specimens [6–11]. The PDE tissue in 1–2 mm³ pieces are cultured *ex vivo* on top of the gelatin sponge, which is half-submerged in medium. This PDE *ex vivo* culture technique maintains cell viability in malignant tissues in their native three-dimensional tissue architecture over culture periods of up to a week. PDE culture of prostate and breast cancers have been shown to faithfully recapitulate the native tumor, to maintain critical molecular driver pathways and allow testing of treatment with therapeutic agents, such as androgen deprivation. Further, these PDE tissues are amenable to whole genome expression analyses, which allow for genetic confirmation of on-target activity and efficacy [12]. The relative technical simplicity, cost-effectiveness and ability to study the heterogeneity of prostate cancer allow for systematic evaluation of therapeutic strategies in prostate cancer.

In this study, we used powerful PDE *ex vivo* culture technique to study DDR of prostate cancer and other solid tumors. Importantly, we identified that the kinetics of DDR in PDEs are significantly faster in PDEs than in cell lines and may reflect better the responses to DNA damage *in vivo*.

\* Corresponding authors at: Department of Urology, University of Texas Southwestern Medical Center, Dallas, TX 75390, USA.
*E-mail addresses:* Ganesh.Raj@utsouthwestern.edu, (G.V. Raj), Yi.Yin@utsouthwestern.edu. (Y. Yin).

## Materials and methods

### Cell lines

Prostate cancer cell line C4-2 was a kind gift from Dr. Leland Chung (Cedar-Sinai Medical Center, Los Angeles, CA) in 2013. Prostate cancer cell lines 22Rv1, LNCaP, PC3, DU145 and breast cancer cell line MDA-MB-231 were purchased directly from ATCC. Cell lines were obtained during 2013–19 and cultures passaged for < 3 months after thawing a given frozen vial. Cells were irradiated using a 137Cs source (Mark 1-68 irradiator; JL Shepherd and Associates) at a dose rate of 3.47 Gy/min.

### Ex vivo cultures of tumor explants

For PDEs, tumor tissues were obtained from patients undergoing surgical resection from University of Texas Southwestern Medical Center (UTSW) and Partners Institution. Tumor samples were processed for *ex vivo* cultures adapting a previously published protocol [12]. Under this protocol, tumor tissues not needed for pathological diagnosis were placed into chilled PBS typically within 30 min of surgical resection and arrived in the laboratory 30–60 min later. Specimens were dissected into approximately 1–2 mm$^3$ pieces and cultured in quadruplicate, as described previously [12]. PDEs were cultured for overnight in the presence and absence of vehicle control (DMSO), enzalutamide (10 μM) or Nu7441 (1 μM). Samples were mock treated or exposed to different doses of IR, followed by 1–48 hour incubation at 37 °C and 5% $CO_2$. Following IR treatments, tumor fragments were then formalin-fixed and paraffin-embedded, snap-frozen, or preserved in RNAlater (Invitrogen, San Diego, CA, USA) depending on the desired downstream analysis. For xenograft derived explants (XDEs), athymic nude mice (nu/nu, 5–6 weeks old) were injected (1 × 10$^6$ cells in 100 μL 50% Matrigel) subcutaneously into the right posterior flanks. Mice were sacrificed when tumor size reached 500 mm$^3$. After excising out the xenografts aseptically from mice, they were cut into 1–2 mm$^3$ tissue fragments and cultured as XDEs in a similar manner to PDEs.

### Immunohistochemistry and immunofluorescent staining

Prostate tissue immunohistochemistry staining for androgen receptor (AR) and prostate-specific antigen (PSA) has been described previously [12]. Tissue fragments were fixed overnight in 10% formalin and placed in embedding cassettes. After, dehydration in 70% ethanol, formalin-fixed tumors were processed using automated standard procedures and subsequently embedded in paraffin. Four-micrometer tissues sections obtained with Leica microtome were mounted on coated microscope slides. For immunofluorescent staining, sections were deparaffinized using xylene and hydrated with declining concentrations of ethanol. Target antigen retrieval was performed using Vector Antigen Retrieval buffer (pH 6.0), which was heated to 100 °C for 20 min. Cells were permeabilized using phosphate buffered saline (PBS) with 0.2% Triton X-100 for 20 min. Blocking was achieved using PBS with 2.5% horse and goat serum. Primary antibodies [anti-p-ATM (abcam ab36801) 1/300, anti-γ-H2AX (Millipore 3292608) 1/300, anti-53BP1 (Novus Biologicals NB100-304) 1/300, anti-p-DNA-PKcs (abcam ab18192) 1/300] were diluted in blocking buffer and incubated over night at 4 °C cold room. Secondary Fluorescein or Texas Red (1/500) antibodies were used to visualize the primary antibody. Sections were mounted using Prolong Gold antifade reagent with DAPi.

### Immunofluorescent analysis

For quantification of DNA damage associated immunofluorescent foci in PDEs, cells with 5 or more foci (to reflect an estimate of induced damage, based on the majority of cells at 0 Gy having 0–4 foci) were scored as positive. The number of cells containing foci (>4) were determined by manually counting 150–200 cells across 4 or more high-power (400×) microscope fields. Percentages of foci–positive cells were calculated at each time point. For foci quantification in XDEs and tumor cell lines, foci numbers again were calculated from at least 150 cells from 4 or more high-power fields at each time point. The number of foci from 150 to 200 cells was counted across multiple microscope fields using Image J (National Institutes of Health). Three independent experiments were performed. Images were acquired with a camera mounted on a Nikon Eclipse E600 fluorescence microscope or Lionheart™ FX Automated Microscope.

### Real-time reverse transcription PCR (qRT-PCR)

RNA was isolated using RNeasy Mini Kit (Qiagen, Valencia, CA) according to the manufacturer's instruction and as previously described [13]. Tissues (0.5–30 mg) preserved in RNAlater (Qiagen, Hilden, Germany) were homogenized with a Precellys 24 Tissue Homogenizer and lysing kit (Bertin Technologies, Montigny-le-Bretonneux, France). Relative quantitation relative to GAPDH expression was calculated by ΔΔCt method following reverse transcription and quantitative real-time PCR as before [13]. qRT-PCR was carried out using specific oligonucleotide primers (Supplementary Table 1).

### Western blotting

Immunoblotting was performed as previously described [13]. Briefly, whole cell or tissue samples were lysed in NP40 extraction buffer containing 50 mmol/L Tris-Cl, pH 7.6, 150 mmol/L NaCl, 5 mmol/L EDTA, 1% NP40, 2 mmol/L dithiothreitol (DTT), 1× Phosphatase Inhibitor Cocktail (Sigma), and 1× Protease Inhibitor Cocktail (Roche). Snap-frozen tissues were homogenized in NP40 extraction buffer with a Precellys 24 Tissue Homogenizer and lysing kit (Bertin Technologies, Montigny-le-Bretonneux, France). 10–30 μg total protein was fractionated by SDS-PAGE and transferred to PVDF membranes (Millipore). Primary antibodies [anti-ATM, anti-p-ATM (abcam ab36801), anti-KAP1 (abcam ab3472), anti-p-KAP1 (phospho S824) antibody (abcam ab70369), anti-CHK2 (Cell Signaling 2662), anti-p-CHK2 (Cell Signaling 2661), anti-p-DNA-PKcs (abcam ab18192), anti-γ-H2AX (Millipore 3292608), anti-β-actin (Cell Signaling), anti-KU80 (abcam ab80592)] were applied followed by horseradish peroxidase-conjugated goat anti-rabbit IgG (H + L) and goat anti-mouse (H + L) (Jackson ImmunoResearch) as secondary antibodies. Pierce™ ECL (Thermal Scientific) or ECL™ prime (GE Healthcare) were used as substrate using the Bio-Rad imaging system.

### Statistics

The statistical results were obtained from at least three independent biological replicates. Detailed n values for each panel in the figures are stated in the corresponding legends. All results were presented as mean ± SEM unless otherwise stated. A 2-tailed unpaired Student's t-test was used to analyze data from experiments containing two groups, while one-way ANOVA was used to analyze data from experiments containing more than two groups. Appropriate posthoc test was used to analyze data that demonstrated significance in ANOVA. $P < 0.05$ was considered to be statistically significant. Statistical analysis was performed using GraphPad Prism 8.0 software.

### Study approval

The de-identified tumor tissues were obtained from patients undergoing surgical resection and the entire study was approved under a protocol approved by the UTSW and Partners Institutional Review Board (IRB) (STU102010-051). All animal experiments were conducted under Institutional Animal Care and Use Committee of UTSW approved guidelines for animal welfare (APN 2016-101380).

## Results

### IR-induced foci formation of DDR proteins in PDE culture of solid tumors

We first evaluated if we could demonstrate the canonical DNA double-strand break (DSB) response to IR in PDE cultures of prostate cancer.

Following IRB approval, we obtained de-identified tumor tissue from patients undergoing a radical prostatectomy at UTSW for clinically localized, National Comprehensive Cancer Network intermediate or high-risk prostate cancer. Tissue cores from these patients were grown using PDE *ex vivo* culture technique, and then subjected to IR or mock treatment. We investigated the induction and decay of IR-induced foci of DDR proteins in distinct prostate cancer PDE using clinically relevant fractional dosage (2 Gy) IR. The DNA damage and the rate of DNA repair were determined using γ-H2AX (Serine 139) and 53BP1 foci staining before and at different time points after IR. The majority of tumor cells in mock treatment control group had 0–4 nuclear γ-H2AX and 53BP1 foci, suggesting a low basal level of DNA damage in treatment-naïve primary tumors (Fig. 1A). We quantified DNA DSB as the number of cells with >4 foci, to reflect an estimate of induced DNA damage. Less than 5% of cells in mock treatment control had >4 nuclear γ-H2AX or 53BP1 foci. In contrast, at 1 h following exposure to 2 Gy IR, the number of cells in irradiated tumor tissues containing γ-H2AX and 53 BP1 foci ranged from 70% to 90% (Fig. 1B), demonstrating recognition of DSBs in prostate cancer PDEs. Importantly, we observed complete resolution of IR-induced γ-H2AX and 53BP1 foci to basal levels within 8 h following exposure to 2 Gy IR, indicating DNA repair kinetics was maintained in prostate cancer PDEs (Fig. 1B). To evaluate the applicability of this PDE culture for other solid tumors, we irradiated fresh surgical
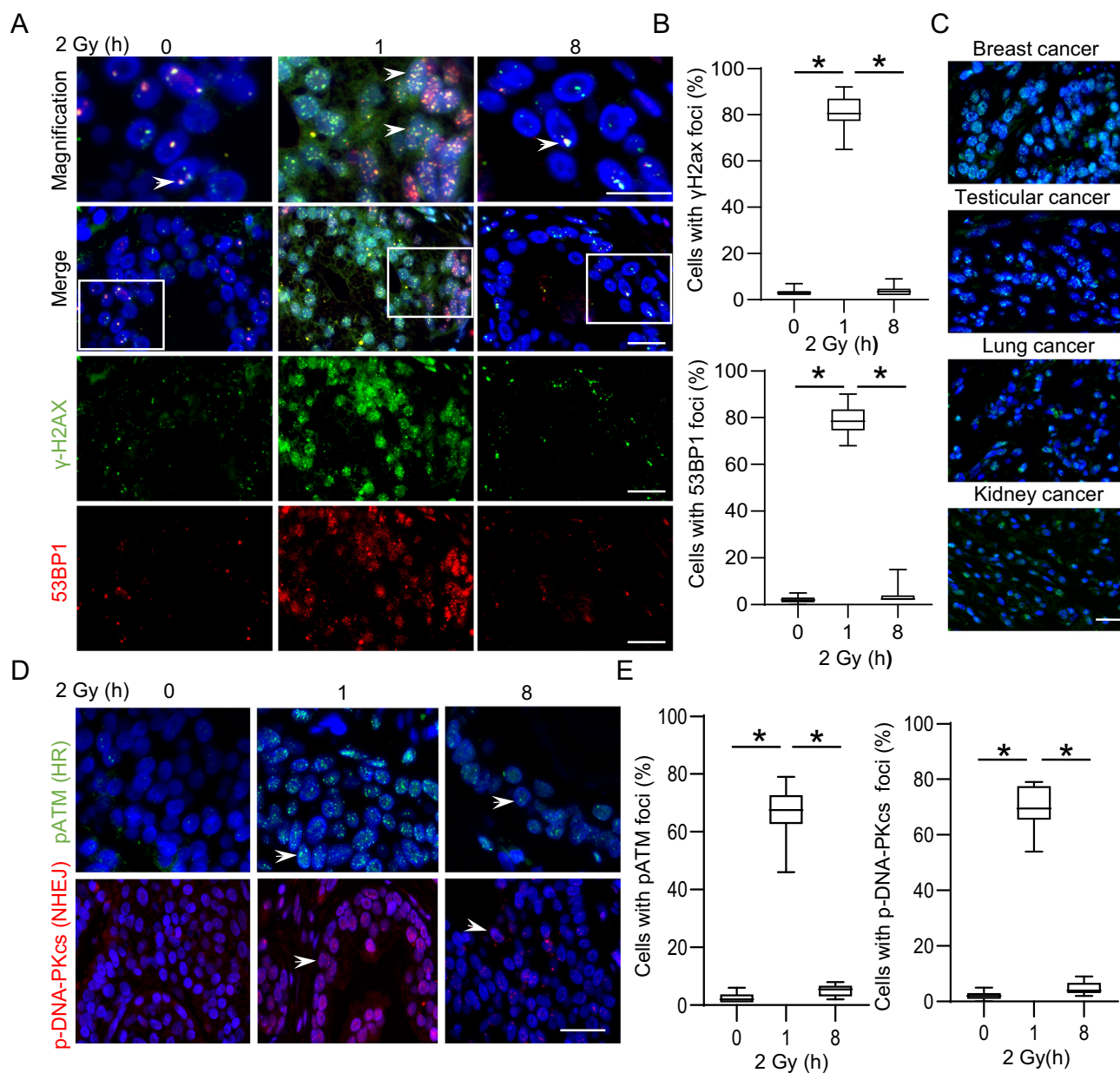


**Fig. 1.** IR-induced foci formation of DDR proteins in PDE culture of solid tumor tissues. PDE culture of solid tumor tissues were radiated with 2 Gy IR and incubated for the indicated times. Tissues were fixed and stained for DDR proteins by immunofluorescence staining. The percentage of foci positive cells was determined by counting at least 150–200 cells per time point from four or more fields of each specimen from 12 patients. A, representative images of γ-H2AX foci (green) and 53 BP1 (red) in the nucleus (blue) of PDE culture of organ-confined prostate cancer before and at 1 and 8 h after IR. White arrow, γ-H2AX and 53BP1 foci. Nuclei were counterstained with DAPi. Top panel of images represent magnifications of cells in white boxes. B, quantification of cells with ≥4 γ-H2AX and 53BP1 foci. C, representative images of γ-H2AX foci (green) in the nucleus (blue) of PDE culture of other types of solid tumors. D, representative images illustrating the induction of p-ATM (blue) and p-DNA-PKcs foci (red) in PDE *ex vivo* culture of prostate cancer incubated for the indicated times following exposure of samples to 2 Gy IR. E, quantification of cells with ≥4 p-ATM and p-DNA-PKcs foci. Scale bar, 50 μm. Box and-whisker plots represent values within the interquartile range (boxes) and the minimum to maximum (whiskers). The line within the box shows the median. *P < 0.001, by 1-way ANOVA with Tukey's multiple comparisons test.

removed treatment-naïve solid tumor tissues obtained from patients with breast, kidney, lung and testicular cancers, cultured as PDEs in a similar manner to prostate cancer. Indeed, we observed similar IR-induced foci formation of DDR proteins and repair kinetics (Fig. 1C).

Mammalian cells have complex mechanisms to repair damaged DNA. IR induced DSBs are repaired by two major competing pathways: error-free homologous recombination (HR), or the error-prone canonical non-homologous end-joining (NHEJ) [14,15]. Since the ataxia telangiectasia mutated (ATM) kinase, the major kinase responsible for modifying γ-H2AX upon irradiation [16], is recruited to and activated primarily at DSBs in conjunction with the MRE11:RAD50:NBS1 (MRN) sensor complex [17], and plays critical role in initiation and completion of error-free HR [18,19], we assessed phospho-ATM (p-ATM) levels following IR in prostate cancer PDEs. IR-induced p-ATM foci (Ser1981) were observed in all 5 tested tumors (Fig. 1D) and may serve as a surrogate for activated HR in prostate cancer PDEs. Similarly, since DNA dependent protein kinase catalytic subunit (DNA-PKcs)'s autophosphorylation in response to DNA damage is a prerequisite for NHEJ, we assessed phospho-DNA-PKcs (p-DNA-PKcs) (Ser2056) levels following IR in prostate cancer PDEs. While basal level of p-DNA-PKcs was low without IR (Fig. 1D), we observed that a rapid induction of p-DNA-PKcs in the epithelial cells within 1 h of 2 Gy IR (Fig. 1D), demonstrating strong activation of DNA-PKcs-mediated NHEJ repair of DSBs. Importantly, these IR-induced p-ATM and p-DNA-PKcs foci also decreased to background levels within 8 h after IR, suggesting that repair of DSBs using both pathways was virtually complete at this stage in *ex vivo* cultures of PDE (Fig. 1E). These results were further validated at the protein level of γ-H2AX, p-ATM, and p-DNA-PKcs by western blots (Supplementary Fig. 1). Consistent with the strong induction of γ-H2AX, p-ATM and p-DNA-PKcs foci, protein levels of γ-H2AX, p-ATM and p-DNA-PKcs increased after 2 Gy radiation but returned to baseline levels at 8 h post-radiation. Together, these data indicate that the PDE system can be used to both follow kinetics of DDR and to delineate specific pathways involved in DDR.

*IR induces distinct DNA damage repair kinetics in prostate cancer PDEs and cell lines*

We compared IR-induced DNA damage repair kinetics in prostate cancer PDE and two well-established prostate cancer cell lines C4-2 and 22Rv1. Although the observed IR-induced foci in prostate cancer PDEs are morphologically similar to IR induced foci seen C4-2 (Fig. 2A) and 22Rv1 (Supplementary Fig. 2A), the repair kinetics in prostate cancer PDEs differ significantly compared with the prostate cancer cell lines. Complete resolution of IR-induced γ-H2AX and 53BP1 foci was observed within 8 h in prostate cancer PDEs (Fig. 1A). In contrast, only 50–60% resolution of foci was observed at 8 h in C4-2 (Fig. 2B) and 22RV1 cell lines (Supplementary Fig. 2B), indicating prostate cancer cell lines have slower DNA repair kinetics in two-dimensional culture.

Given that tumor microenvironment and tumor-stromal interactions produce profound changes in tumor phenotype [20], we next sought to determine whether these factors in *ex vivo* cultured explants would reduce or augment DDR induced by IR. We reasoned that if prostate cancer cell lines were allowed to form xenograft tumors in mice and tested as explants, they would then exhibit distinctive responses to radiation than they did in two-dimensional culture, due to the influence of the tumor-stromal interactions on DDR within the tumor microenvironments. To this end, xenograft derived explants (XDEs) were developed using mouse xenograft tumors grown from the prostate cancer C4-2 cell line. Tissue fragments derived from C4-2 XDEs were cultured and irradiated *ex vivo* as PDE culture of solid tumors. The foci were analyzed after different time points after 2 Gy IR to assess the induction of DSBs as well as repair kinetics responses. We observed similar number of foci 30 min post 2 Gy in C4-2 XDEs compared to cell lines in two-dimensional *ex vivo* culture (Fig. 2C), indicating tumor microenvironment and tumor-stromal interactions have limited impact on initial DNA damage induction. In contrast, we observed a significantly faster rate of DSB repair in XDEs compared with two-dimensionally

cultured C4-2 cells (Fig. 2B). More than 90% repair was completed at 8 h following IR in C4-2 XDEs (Fig. 2C and D), whereas two-dimensional cultured C4-2 cells still retained nearly 50%, 30% and 10% of foci at 8, 16 and 24 h, respectively (Fig. 2B), suggesting that the tumor-stromal interactions potentially promote DNA repair in tumor explants. Similarly, complete foci resolution was observed within 8 h in breast cancer MDA-MD-231 XDEs (Supplementary Fig. 3A and B), but not in two-dimensionally cultured MDA-MD-231 cells (Supplementary Fig. 3C and D). This result was further validated in C4-2 cells and C4-2 XDEs at the protein level of γ-H2AX by western blots (Fig. 2E). Consistent with the studies of others [21,22], the presented results suggest that tumor-stromal interactions would likely influence radiation-induced DDR of tumor cells. All these results imply that the kinetics of DNA damage-related proteins at DNA lesions can vary among different microenvironments.

*IR induces a distinct transcriptional program in prostate cancer PDE and cell lines*

We assessed time and dose-dependent association between IR and IR induced transcriptional changes of a panel of DDR genes in PDEs by RT q-PCR. We observed a time and dose-dependent response to IR, with a maximum effect noted around 4 h at 2 Gy (Supplementary Fig. 4A and B). We measured the expression level of a panel of canonical DDR related genes (RAD21, RAD51, RAD54B, DNA PKc, KU70, XRCC4, XRCC5, CHK1, CHK2, ATM, ATR, and P21) in 12 prostate cancer PDEs and multiple cancer cell lines by RT q-PCR at 4 h after 2 Gy IR. Significant upregulation in the expression of all tested DDR-related genes were noted in prostate cancer PDEs (Fig. 3A). As would be expected with tumor heterogeneity, the fold change at 4 h for some of these DDR-related genes varied greatly between individual tumors. In contrast, majority (>90%) of these canonical DDR genes are not significantly induced following 2 Gy IR of prostate cancer (C4-2, 22RV1, DU145 and PC3) and breast cancer (MDA-MD-231) cell lines (Fig. 3B and Supplementary Fig. 5). In these cell lines, we only observed significant upregulation <50% of these canonical DDR-related genes even after high-doses of RT (10 Gy). To document DDR signaling following exposure to IR, we measured the expression levels of total and phosphorylated ATM, KAP1, and CHK2 by immunoblotting in prostate cancer PDE and two representative prostate cancer cell lines (C4-2 and 22Rv1). Total ATM, KAP1, and CHK2 did not vary significantly in PDE and cancer cell lines (Fig. 3C and D). 2 Gy IR induced classic DDR signaling including the phosphorylation of ATM at position Ser1981, KAP1 at position Ser824 and Chk2 at position Thr68 in PDE (Fig. 3C). Relative to the vehicle control, high-doses of IR (10 Gy) induced classic DDR signaling including the phosphorylation of ATM at position Ser1981, KAP1 at position Ser824, and CHK2 at position Thr68 in these prostate cancer cell lines. In contrast, the 2 Gy IR induced modest increases in phosphorylation of ATM at position Ser1981 and KAP1 at position Ser824 in C4-2 cells, and did not result in altered phosphorylation of KAP1 at position Ser824 and CHK2 at position Thr68 in 22Rv1 cells, which may in part explain the slower kinetics of DDR responses in cancer cell lines (Fig. 3D).

*DNA-PKcs inhibition blocks IR-induced DDR in prostate cancer PDE*

We had shown that the DNA-PKcs inhibitor (Nu7441) sensitizes prostate cancer to IR in prostate cancer cell lines [13]. We next sought to determine whether inhibition of DNA-PKcs would reduce or augment DNA damage induced by IR in prostate cancer PDEs. Treatment of prostate cancer PDEs with Nu7441 significantly attenuated the p-DNA-PKcs (pS2056) foci resulting from IR exposure (Fig. 4A), indicating target engagement. Pretreatment of the prostate cancer PDEs with Nu7441 for 24 h did not affect the basal level of DNA damage as evidenced by the similar number of γ-H2AX foci in both Nu7441 and vehicle control treated PDEs (Fig. 4B and Supplementary Fig. 6). Importantly, at 1 h after IR, pretreatment of prostate cancer PDE with Nu7441 did not affect the DNA damage caused by IR, as evidenced by the similar number of γ-H2AX and 53BP1 foci in both Nu7441 and vehicle control treated PDEs (Fig. 4B). Further, at 8 h after IR, pretreatment with Nu7441 substantially reduced nuclear γ-H2AX foci
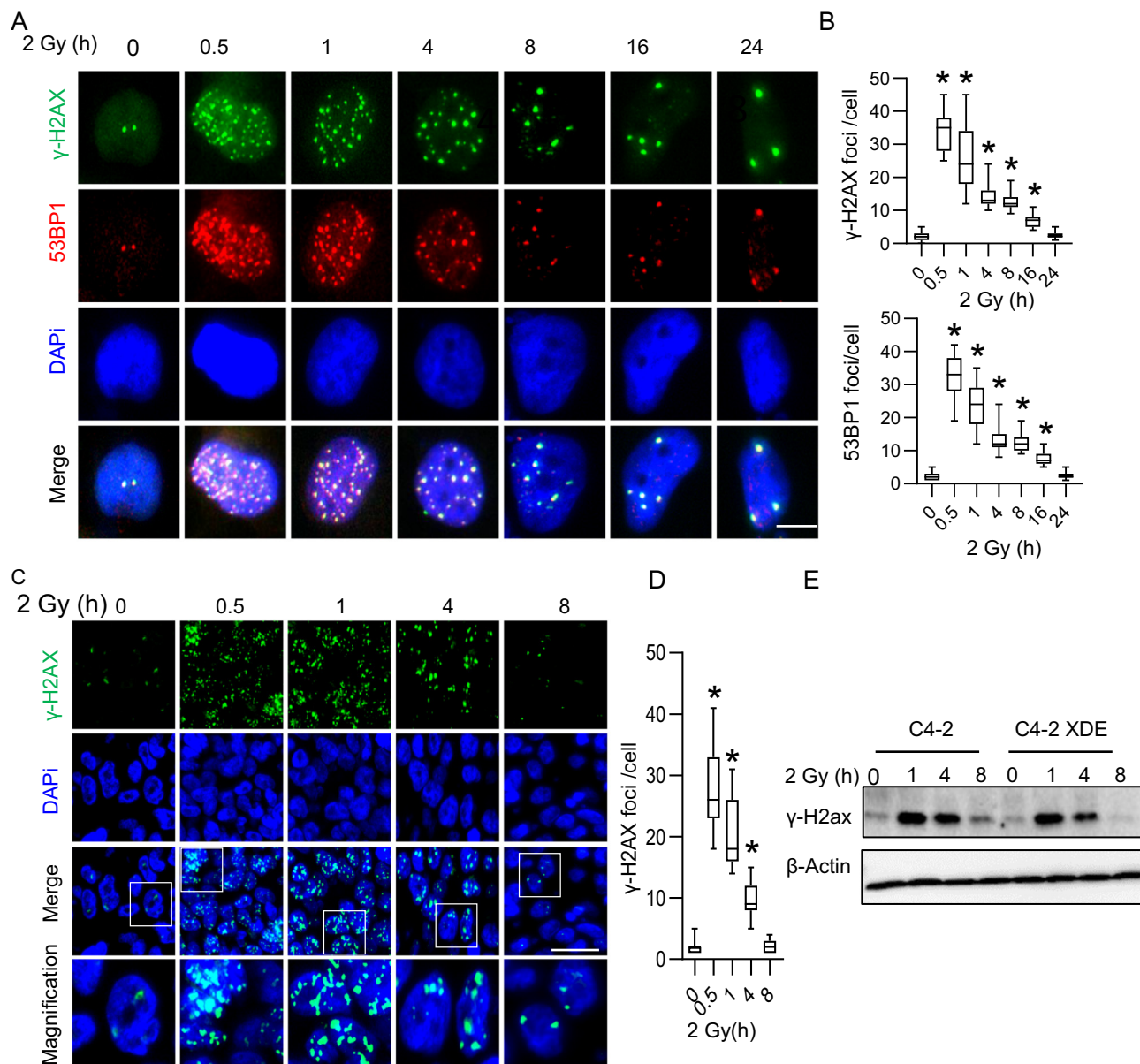
**Fig. 2.** IR-induced foci formation of DDR proteins in prostate cancer cells and XDE. C4-2 prostate cancer cells and C4-2 XDE were radiated with 2 Gy and incubated for the indicated times. A, Cells and tissues were fixed and stained for DNA damage repair proteins by immunofluorescence staining. Representative images of γ-H2AX foci (green) and 53 BP1 (red) in the nucleus (blue) of cultured C4–2 cells at indicated time points after irradiation with a dose of 2 Gy (scale bar, 10 μm). B, the number of foci per cell was determined by counting at least 200 cells per experiment. C, representative images of γ-H2AX foci (green) in the nucleus (blue) of C4–2 XDE at indicated time points after irradiation with a dose of 2 Gy. Bottom panel of images represent enlargements of cells in white boxes (scale bar, 50 μm). D, the number of foci per foci-positive cell was determined by counting at least 150 cells per experiment. Box and-whisker plots represent values within the interquartile range (boxes) and the minimum to maximum (whiskers). The line within the box shows the median. *P < 0.001 *vs.* control, by 1-way ANOVA with Tukey's multiple comparisons test. E, Western blot detection of γ-H2ax in C4-2 cells and C4-2 XDE at indicated time points after irradiation with a dose of 2 Gy.

resolution. Consistent with γ-H2AX foci staining, we observed similar result at protein levels of γ-H2AX by western blot (Supplementary Fig. 7), supporting previous studies demonstrating the role for DNA-PKcs enhancing DDR in prostate cancer [23]. While these data corroborate the role of DNA-PKcs in both prostate cancer PDEs and cell lines, the altered kinetics of repair are still noteworthy.

*Inhibition of AR impairs NHEJ in prostate cancer PDEs*

Given that AR plays a critical role in repairing of radiation-induced potentially lethal DSBs in prostate cancer, and PDE *ex vivo* culture sustains endocrine signaling and therapeutic response to established clinical agents [12], we sought to confirm that combining the second-generation AR

inhibitor enzalutamide with IR impairs repair of DSBs. We first confirmed that pretreatment of the prostate cancer PDEs with enzalutamide (10 μM) for 24 h attenuated the AR signaling, as evidenced by reduced AR and PSA expression (Fig. 5A). Pretreatment of prostate cancer PDE with enzalutamide did not affect the DNA damage caused by IR, as evidenced by the similar number of γ-H2AX and 53BP1 foci in both enzalutamide and vehicle control treated PDEs (Fig. 5B). However, in the presence of enzalutamide, γ-H2AX and 53BP1 foci were persistent for up to 48 h after 2 Gy IR (Fig. 5B and C). Further evaluation indicates that the NHEJ pathway is influenced by enzalutamide, as shown by the significantly decreased ability of IR to induce p-DNA-PKcs foci in enzalutamide treated prostate cancer PDEs *versus* vehicle-treated controls (Fig. 5D and E). These data build on prior observations from prostate cancer cell lines that AR

**A**



**C**



**B**



**D**
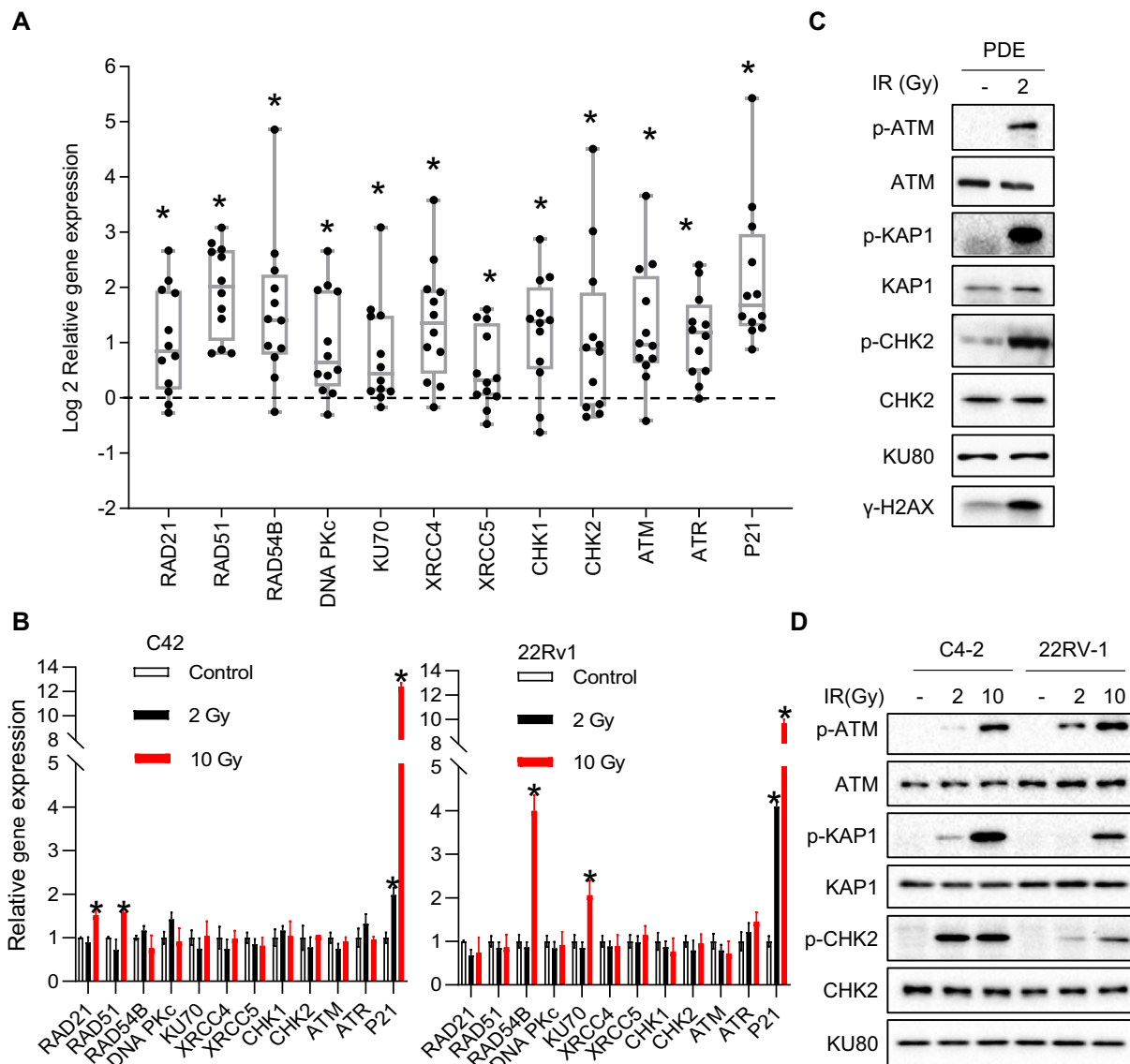


**Fig. 3.** IR-induced DDR related genes transcriptional and signaling changes in PDE culture of prostate cancer and two-dimensional cultured cancer cell lines. PDE culture of prostate cancer and two-dimensional culture of cancer cells were treated with no IR or radiated with 2 Gy and incubated for 4 h. A, individual variation in gene expression response to clinic relevant dose IR in PDEs derived from 12 prostate cancer patients following IR. Dots represent fold-change values of indicated gene in each patient sample. Box and-whisker plots represent values within the interquartile range (boxes) and the minimum to maximum (whiskers). The line within the box shows the median. On the y axis, a fold change log 2 value of 0 (horizontal dash line) corresponds to no difference in expression levels between IR and control group. For log 2 values plotted above 0, mRNA abundance in IR is higher than in control. For log2 values plotted below 0, mRNA abundance in IR is lower than in control. B, DDR gene expression response to 2 Gy IR in prostate cancer cell lines (C4-2, 22Rv1) in two-dimensional culture. *P < 0.05 *vs.* control, by Student's *t*-test. C, Immunoblot analyses of the indicated proteins in PDE culture of prostate cancer. D, Immunoblot analyses of the indicated proteins in prostate cancer cell lines.

inhibition may regulate DNA repair through a DNA PK-dependent mechanism [24], and indicate that the repair kinetics with these drugs is significantly prolonged in PDEs rather than in cell lines.

## Discussion

Understanding DDR of primary cancer cells is important to developing strategies for overcoming radiation resistance and enabling better outcomes for patients undergoing radiation therapy. In this manuscript, we have shown that PDEs of multiple primary tumors can server as a clinically relevant model to study the biological effects of IR on primary cancers. In primary localized prostate cancer PDEs, we have noted DNA damage, transcriptional changes, engagement of specific DDR signaling pathways and kinetics of DNA repair following 2 Gy IR. We have seen that the DNA repair kinetics are much faster in PDEs of primary prostate cancer rather than in

cancer cell lines, indicating a role for the stromal microenvironment in facilitating DDR: impressively, we have noted distinct repair kinetics in a cancer cell line cultured *in vitro* and the same cell line cultured as a XDE from a xenograft. Our study strongly indicates a significant influence of the tumor stroma on the DDR response to radiation therapy.

One of the great challenges in cancer treatment is the individual variation in response to therapy. Similarly, we observed wide variation in IR-induced transcription of DDR related genes in PDE tissues, reflecting the diverse genetic heterogeneity of prostate tumors. In contrast, established tumor cell lines and genetically engineered mouse models do not represent the variation and heterogeneity observed in cancers from patients. More importantly, all commercially available prostate cancer cell lines are derived from metastatic deposits of prostate cancer and therefore might not accurately reflect cellular response in primary prostate cancer, as there is substantial evidence for altered expression profiles of androgen-regulated
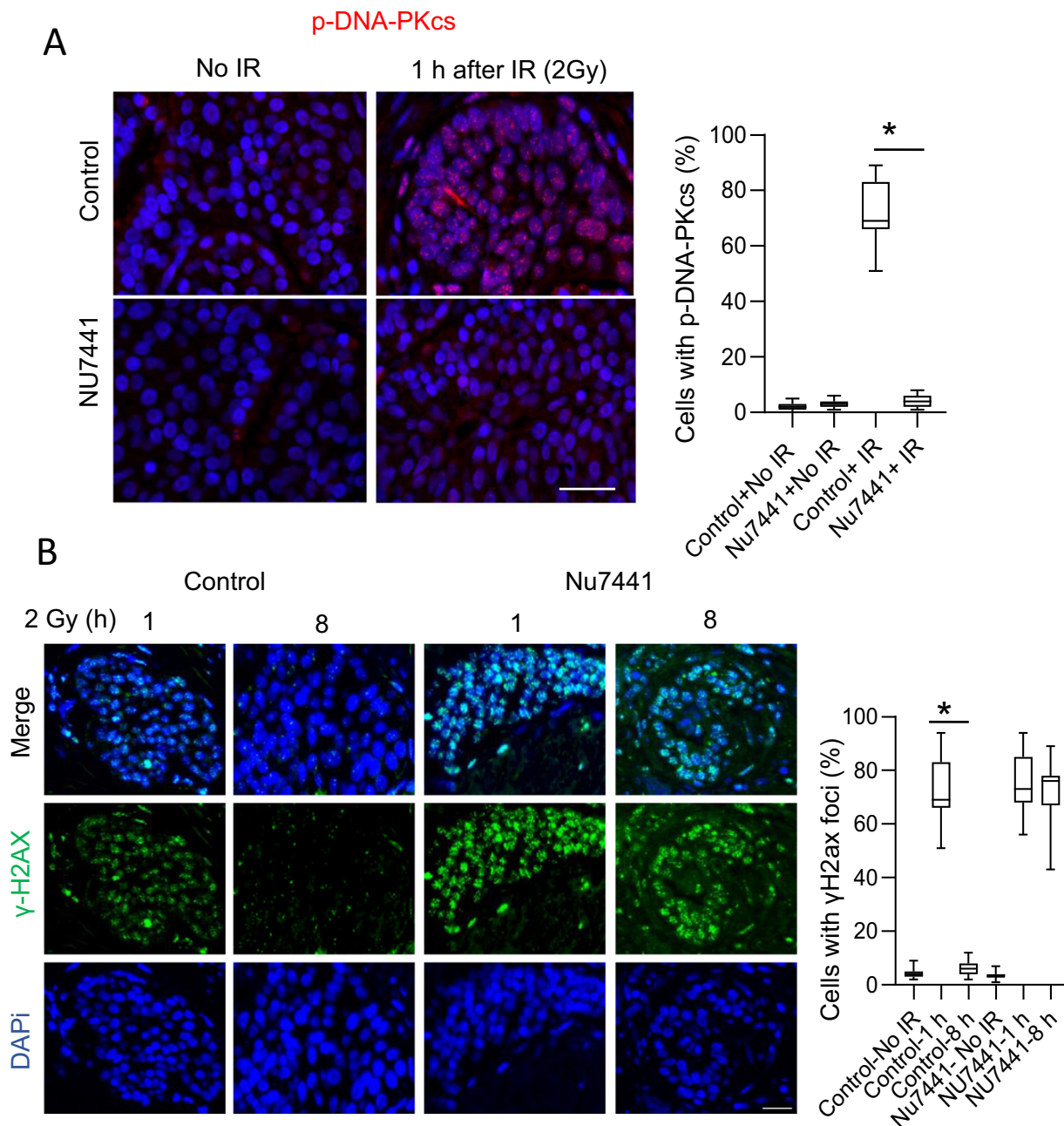
**Fig. 4.** DNA-PKcs inhibition blocks IR-induced DDR in PDE culture of prostate cancer. PDE culture of prostate cancer tissues were incubated with Nu7441 (1 μM) or vehicle control (DMSO) for 24 h, and then radiated with 0 or 2 Gy and incubated for the indicated times. A, tissues were fixed and stained for p-DNA-PKcs. Representative images (left) and quantification (right) of cells with p-DNA-PKcs were shown. B, Tissues were fixed and stained for γ-H2AX (green) by immunofluorescence staining. Representative images (left) and quantification (right) of cells with γ-H2AX were shown. The percentage of foci positive cells was determined by counting at least 150 cells per time point from three to four fields of each specimen from 5 patients. Box and-whisker plots represent values within the interquartile range (boxes) and the minimum to maximum (whiskers). The line within the box shows the median. *P < 0.001, by 1-way ANOVA with Tukey's multiple comparisons test. Scale bar, 50 μm.

genes in metastatic *versus* primary prostate cancer [25,26]. Recently, the development of organoid cultures from advanced metastatic heavily pretreated prostate cancer specimens provides new tools for evaluating therapies and making important discoveries [27,28]. However, culturing prostate organoids from localized, treatment-naïve organ-confined prostate cancer has not proven feasible. In part, the derivation of organoids from localized prostate cancer may be limited by current protocols for organoid culture which are focused on epithelial cells and do not include other cells of the tumor microenvironment such as stroma, immune, and neuronal cell populations [29]. For the determination of DNA repair of human cancer cells, an *ex vivo* approach can provide a more accurate result compared with *in vitro* cell cultures, since the

DNA repair ability is measured directly without the influence of prolonged culture time.

The primary advantage of the PDE approach is that it enables rapid evaluation of the effect of IR on primary tumors- the very tumors that would be treated with radiation therapy. The primary limitation of this approach may be related to the heterogeneity of solid tumors, which may complicate the data interpretation. The utility of PDEs as a surrogate for tumor response is not proven and does not adequately address the role of the immune system in mediating RT response. However, the *ex vivo* culture systems recapitulate the structural complexity and heterogeneity of human solid tumors in a laboratory setting, making them an important adjunct to current cell-line-based and animal-based models. We have validated our published data
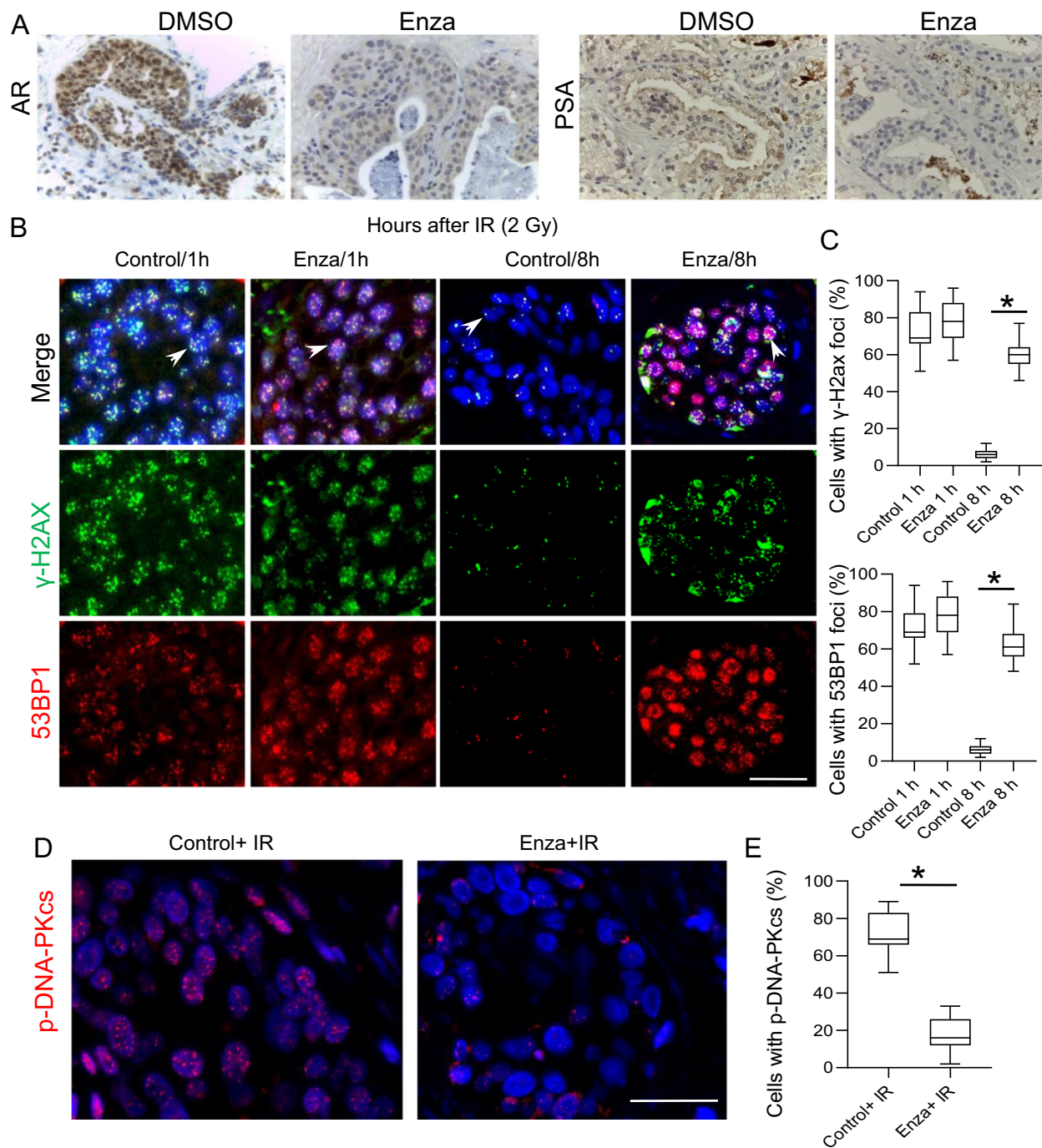
**Fig. 5.** Inhibition of AR impairs NHEJ in PDE culture of organ-confined prostate cancer. A, PDE culture of prostate cancer tissues were incubated with enzalutamide (10 μM) or vehicle control (DMSO) for 24 h, tissues were fixed and stained for AR and PSA. Representative images of AR and PSA were shown. B, PDE culture of prostate cancer tissues were pretreated with enzalutamide (10 μM) or control (DMSO) for 24 h and then radiated with 2 Gy and incubated for the indicated times. Tissues were fixed and stained for γ-H2AX (green) and 53BP1 (red) by immunofluorescence staining. C, quantification of cells with γ-H2AX (left) and 53BP1 (right) foci. The percentage of foci positive cells was determined by counting at least 150 cells per time point from three to four fields of each specimen from 5 patients. *P < 0.001, by 1-way ANOVA with Tukey's multiple comparisons test. D, PDE culture of prostate cancer tissues were pretreated with enzalutamide for 24 h and then radiated with 2 Gy and incubated for 1 h. Tissues were fixed and stained for p-DNA-PKcs (red) by immunofluorescence staining. E, quantification of cells with p-DNA-PKcs foci. Box and-whisker plots represent values within the interquartile range (boxes) and the minimum to maximum (whiskers). The line within the box shows the median. *P < 0.001, by unpaired Student *t*-test. Scale bar, 50 μm.

indicated that AR inhibition and DNA-PKc inhibition sensitized prostate cancer cells to radiotherapy in primary tumors using our *ex vivo* cultures [13]. These data indicate that inhibition of DNA-PKc and AR acts similarly in prostate cancer cell lines, PDEs and XDEs and strongly suggest that drugs targeting AR and/or DNA-PKc may enhance the utility of radiation in patients with prostate cancer.

Taken together, PDEs enables short-term evaluation of DDR in primary solid tumors in their clinically relevant microenvironment, and enable evaluation of the utility of DDR modulators for PDEs. These PDEs show a distinct repair kinetics than cell lines, and may offer a more biologically relevant model for studying DDR responses in prostate cancer.

Supplementary data to this article can be found online at https://doi.org/10.1016/j.tranon.2020.100898.

## CRediT authorship contribution statement

Collin Gilbreath: Methodology, Validation, Formal analysis, Investigation. Shihong Ma: Methodology, Validation, Formal analysis, Investigation. Lan Yu: Methodology, Validation, Formal analysis, Investigation. Rajni Sonavane: Methodology, Validation, Formal analysis, Investigation. Carlos M. Roggero: Investigation. Anvita Devineni: Investigation. Ryan Mauck: Resources. Neil B. Desai: Resources, Writing - review & editing. Aditya Bagrodia: Resources. Ralf Kittler: Conceptualization, Writing - review & editing. Ganesh V. Raj: Conceptualization, Methodology, Validation, Formal analysis, Investigation, Writing - review & editing, Supervision, Project administration, Funding acquisition. Yi Yin: Conceptualization, Methodology, Validation, Formal analysis, Investigation, Writing - original draft, Supervision, Writing - review & editing, Project administration, Funding acquisition. All authors discussed results and approved the final manuscript.

## Declaration of competing interest

The authors declare that they have no known competing financial interests or personal relationships that could have appeared to influence the work reported in this paper.

## Acknowledgments

## References

[1] Pienta KJ, Abate-Shen C, Agus DB, Attar RM, Chung LW, Greenberg NM, Hahn WC, Isaacs JT, Navone NM, Peehl DM, Simons JW, Solit DB, Soule HR, VanDyke TA, Weber MJ, Wu L, Vessella RL. The current state of preclinical prostate cancer animal models. Prostate. 2008;68(6):629–39. Epub 2008/01/24. doi:https://doi.org/10.1002/pros.20726. PubMed PMID: 18213636; PMCID: 3681409.

[2] R. Toivanen, R.A. Taylor, D.W. Pook, S.J. Ellem, G.P. Risbridger, Breaking through a roadblock in prostate cancer research: an update on human model systems, J. Steroid Biochem. Mol. Biol. 131 (3–5) (2012) 122–131, Epub 2012/02/22 https://doi.org/10.1016/j.jsbmb.2012.01.00522342674.

[3] S.J. Ellem, E.M. De-Juan-Pardo, G.P. Risbridger, In vitro modeling of the prostate cancer microenvironment, Adv. Drug Deliv. Rev. (2014)https://doi.org/10.1016/j.addr.2014.04.00824816064.

[4] T. Criswell, K. Leskov, S. Miyamoto, G. Luo, D.A. Boothman, Transcription factors activated in mammalian cells after clinically relevant doses of ionizing radiation, Oncogene. 22 (37) (2003) 5813–5827, https://doi.org/10.1038/sj.onc.120668012947388.

[5] S.B. Shappell, G.V. Thomas, R.L. Roberts, R. Herbert, M.M. Ittmann, M.A. Rubin, P.A. Humphrey, J.P. Sundberg, N. Rozengurt, R. Barrios, J.M. Ward, R.D. Cardiff, Prostate pathology of genetically engineered mice: definitions and classification. The consensus report from the Bar Harbor meeting of the Mouse Models of Human Cancer Consortium Prostate Pathology Committee, Cancer Res. 64 (6) (2004) 2270–2305, Epub 2004/03/18 15026373.

[6] M.M. Centenera, G.V. Raj, K.E. Knudsen, W.D. Tilley, L.M. Butler, Ex vivo culture of human prostate tissue and drug development, Nat. Rev. Urol. 10 (8) (2013) 483–487, Epub 2013/06/12 https://doi.org/10.1038/nrurol.2013.12623752995.

[7] P. Ravindranathan, T.K. Lee, L. Yang, M.M. Centenera, L. Butler, W.D. Tilley, J.T. Hsieh, J.M. Ahn, G.V. Raj, Peptidomimetic targeting of critical androgen receptor-coregulator interactions in prostate cancer, Nat. Commun. 4 (2013) 1923, Epub 2013/05/30 https://doi.org/10.1038/ncomms291223715282.

[8] Sen A, De Castro I, Defranco DB, Deng FM, Melamed J, Kapur P, Raj GV, Rossi R, Hammes SR. Paxillin mediates extranuclear and intranuclear signaling in prostate cancer proliferation. J Clin Invest. 2012;122(7):2469–81. Epub 2012/06/12. doi:https://doi.org/10.1172/JCI62044. PubMed PMID: 22684108; PMCID: 3386821.

[9] M.M. Centenera, J.L. Gillis, A.R. Hanson, S. Jindal, R.A. Taylor, G.P. Risbridger, P.D. Sutherland, H.I. Scher, G.V. Raj, K.E. Knudsen, T. Yeadon, W.D. Tilley, L.M. Butler, Evidence for efficacy of new Hsp90 inhibitors revealed by ex vivo culture of human prostate tumors, Clin. Cancer Res. 18 (13) (2012) 3562–3570, Epub 2012/05/11 https://doi.org/10.1158/1078-0432.CCR-12-078222573351.

[10] Schiewer MJ, Goodwin JF, Han S, Brenner JC, Augello MA, Dean JL, Liu F, Planck JL, Ravindranathan P, Chinnaiyan AM, McCue P, Gomella LG, Raj GV, Dicker AP, Brody JR, Pascal JM, Centenera MM, Butler LM, Tilley WD, Feng FY, Knudsen KE. Dual roles of PARP-1 promote cancer growth and progression. Cancer discovery. 2012;2(12):1134–49. Epub 2012/09/21. doi:https://doi.org/10.1158/2159-8290.CD-12-0120. PubMed PMID: 22993403; PMCID: PMC3519969.

[11] Wang S, Kollipara RK, Srivastava N, Li R, Ravindranathan P, Hernandez E, Freeman E, Humphries CG, Kapur P, Lotan Y, Fazli L, Gleave ME, Plymate SR, Raj GV, Hsieh JT, Kittler R. Ablation of the oncogenic transcription factor ERG by deubiquitinase inhibition in prostate cancer. Proc Natl Acad Sci U S A. 2014;111(11):4251–6 Epub 2014/03/05. doi:https://doi.org/10.1073/pnas.1322198111. PubMed PMID: 24591637; PMCID: PMC3964108.

[12] Centenera MM, Hickey TE, Jindal S, Ryan NK, Ravindranathan P, Mohammed H, Robinson JL, Schiewer MJ, Ma S, Kapur P, Sutherland PD, Hoffmann CE, Roehrborn CG, Gomella LG, Carroll JS, Birrell SN, Knudsen KE, Raj GV, Butler LM, Tilley WD. A patient-derived explant (PDE) model of hormone-dependent cancer. Mol Oncol. 2018;12(9):1608–22. Epub 2018/08/18. doi:https://doi.org/10.1002/1878-0261.12354. PubMed PMID: 30117261; PMCID: PMC6120230.

[13] Yin Y, Li R, Xu K, Ding S, Li J, Baek G, Ramanand SG, Ding S, Liu Z, Gao Y, Kanchwala MS, Li X, Hutchinson R, Liu X, Woldu SL, Xing C, Desai NB, Feng FY, Burma S, de Bono JS, Dehm SM, Mani RS, Chen BPC, Raj GV. Androgen receptor variants mediate DNA repair after prostate cancer irradiation. Cancer Res. 2017;77(18):4745–54. Epub 2017/07/30. doi:https://doi.org/10.1158/0008-5472.CAN-17-0164. PubMed PMID: 28754673; PMCID: PMC5600864.

[14] D. Branzei, M. Foiani, Regulation of DNA repair throughout the cell cycle, Nat. Rev. Mol. Cell. Biol. 9 (4) (2008) 297–308, Epub 2008/02/21 https://doi.org/10.1038/nrm235118285803.

[15] Jackson SP, Bartek J. The DNA-damage response in human biology and disease. Nature. 2009;461(7267):1071–8. Epub 2009/10/23. doi:https://doi.org/10.1038/nature08467. PubMed PMID: 19847258; PMCID: PMC2906700.

[16] S. Burma, B.P. Chen, M. Murphy, A. Kurimasa, D.J. Chen, ATM phosphorylates histone H2AX in response to DNA double-strand breaks, J. Biol. Chem. 276 (45) (2001) 42462–42467, Epub 2001/09/26 https://doi.org/10.1074/jbc.C10046620011571274.

[17] J.H. Lee, T.T. Paull, ATM activation by DNA double-strand breaks through the Mre11-Rad50-Nbs1 complex, Science. 308 (5721) (2005) 551–554, Epub 2005/03/26 https://doi.org/10.1126/science.110829715790808.

[18] Ahlskog JK, Larsen BD, Achanta K, Sorensen CS. ATM/ATR-mediated phosphorylation of PALB2 promotes RAD51 function. EMBO Rep. 2016;17(5):671–81. Epub 2016/04/27. doi:10.15252/embr.201541455. PubMed PMID: 27113759; PMCID: PMC5341514.

[19] Bakr A, Oing C, Kocher S, Borgmann K, Dornreiter I, Petersen C, Dikomey E, Mansour WY. Involvement of ATM in homologous recombination after end resection and RAD51 nucleofilament formation. Nucleic Acids Res. 2015;43(6):3154–66. Epub 2015/03/11. doi:https://doi.org/10.1093/nar/gkv160. PubMed PMID: 25753674; PMCID: PMC4381069.

[20] R. Kalluri, The biology and function of fibroblasts in cancer, Nat. Rev. 16 (9) (2016) 582–598, Epub 2016/08/24 https://doi.org/10.1038/nrc.2016.7327550820.

[21] Ketteler J, Panic A, Reis H, Wittka A, Maier P, Herskind C, Yague E, Jendrossek V, Klein D. Progression-related loss of stromal caveolin 1 levels mediates radiation resistance in prostate carcinoma via the apoptosis inhibitor TRIAP1. J Clin Med. 2019;8(3). Epub 2019/03/16. doi:https://doi.org/10.3390/jcm8030348. PubMed PMID: 30871022; PMCID: PMC6462938.

[22] Steer A, Cordes N, Jendrossek V, Klein D. Impact of cancer-associated fibroblast on the radiation-response of solid xenograft tumors. Front Mol Biosci. 2019;6:70. Epub 2019/09/03. doi:https://doi.org/10.3389/fmolb.2019.00070. PubMed PMID: 31475157; PMCID: PMC6705217.

[23] Goodwin JF, Schiewer MJ, Dean JL, Schrecengost RS, de Leeuw R, Han S, Ma T, Den RB, Dicker AP, Feng FY, Knudsen KE. A hormone-DNA repair circuit governs the response to genotoxic insult. Cancer discovery. 2013;3(11):1254–71. Epub 2013/09/13. doi:https://doi.org/10.1158/2159-8290.CD-13-0108. PubMed PMID: 24027197; PMCID: PMC3823813.

[24] Tarish FL, Schultz N, Tanoglidi A, Hamberg H, Letocha H, Karaszi K, Hamdy FC, Granfors T, Helleday T. Castration radiosensitizes prostate cancer tissue by impairing DNA double-strand break repair. Science translational medicine. 2015;7(312):312re11. Epub 2015/11/06. doi:https://doi.org/10.1126/scitranslmed.aac5671. PubMed PMID: 26537259.

[25] Nevedomskaya E, Stelloo S, van der Poel HG, de Jong J, Wessels LF, Bergman AM, Zwart W. Androgen receptor DNA binding and chromatin accessibility profiling in prostate cancer. Genom Data. 2016;7:124–6. Epub 2016/03/17. doi:https://doi.org/10.1016/j.gdata.2015.12.020. PubMed PMID: 26981385; PMCID: PMC4778643.

[26] Labbe DP, Brown M. Transcriptional regulation in prostate cancer. Cold Spring Harb Perspect Med. 2018;8(11). Epub 2018/03/14. doi:https://doi.org/10.1101/cshperspect.a030437. PubMed PMID: 29530947.

[27] Gao D, Vela I, Sboner A, Iaquinta PJ, Karthaus WR, Gopalan A, Dowling C, Wanjala JN, Undvall EA, Arora VK, Wongvipat J, Kossai M, Ramazanoglu S, Barboza LP, Di W, Cao Z, Zhang QF, Sirota I, Ran L, MacDonald TY, Beltran H, Mosquera JM, Touijer KA, Scardino PT, Laudone VP, Curtis KR, Rathkopf DE, Morris MJ, Danila DC, Slovin SF, Solomon SB, Eastham JA, Chi P, Carver B, Rubin MA, Scher HI, Clevers H, Sawyers CL, Chen Y. Organoid cultures derived from patients with advanced prostate cancer. Cell. 2014;159(1):176–87. Epub 2014/09/10. doi:https://doi.org/10.1016/j.cell.2014.08.016. PubMed PMID: 25201530; PMCID: PMC4237931.

[28] Drost J, Karthaus WR, Gao D, Driehuis E, Sawyers CL, Chen Y, Clevers H. Organoid culture systems for prostate epithelial and cancer tissue. Nat Protoc. 2016;11(2):347–58. Epub 2016/01/23. doi:https://doi.org/10.1038/nprot.2016.006. PubMed PMID: 26797458; PMCID: PMC4793718.

[29] Risbridger GP, Toivanen R, Taylor RA. Preclinical models of prostate cancer: patient-derived xenografts, organoids, and other explant models. Cold Spring Harb Perspect Med. 2018;8(8). Epub 2018/01/10. doi:https://doi.org/10.1101/cshperspect.a030536. PubMed PMID: 29311126.